

Electronic Supplementary Material (ESI) for Journal of Materials Chemistry A.
This journal is © The Royal Society of Chemistry 2023

Electronic Supporting Information

**Enhancing of selective conversion of nitrate electrochemical via π back-donation
on Lewis acid sites induced by noble-metal doping CoP**

Yihong Gao,^a Kunpeng Wang,^a Shikuo Li,^{* b} Hui Zhang, ^{* b} Fangzhi Huang,^{* a}

^aSchool of Chemical and Chemical Engineering, Anhui University, Hefei, Anhui
230601, China

^bSchool of Material Science and Engineering, Anhui University, Hefei, Anhui 230601,
China

Corresponding author:

Prof. Shikuo Li, E-mail: lishikuo@ahu.edu.cn

Prof. Hui Zhang, E-mail: zhui@ahu.edu.cn

Prof. Fangzhi Huang, E-mail: huangfangzhi@163.com

Experiment section

1.1 Chemicals

Ti mesh (1 mm thickness) was purchased from Kangwei department (Dalian, PR China). Cobalt nitrate hexahydrate ($\text{Co}(\text{NO}_3)_2 \cdot 6\text{H}_2\text{O}$), Urea ($\text{CO}(\text{NH}_2)_2$), Ammonium fluoride (NH_4F), Sodium tetrachloropalladium (Na_2PdCl_4) and Sodium hypophosphite monohydrate ($\text{NaH}_2\text{PO}_2 \cdot \text{H}_2\text{O}$) were purchased from Sigma-Aldrich. ammonium sulfate- ^{14}N ($(^{14}\text{NH}_4)_2\text{SO}_4$, 98.5 %), ammonium sulfate- ^{15}N ($(^{15}\text{NH}_4)_2\text{SO}_4$, ≥ 99 at%, 98.5 %), sodium nitrate- ^{14}N ($\text{Na}^{14}\text{NO}_3$, 98.5 %), sodium nitrate- ^{15}N ($\text{Na}^{15}\text{NO}_3$, $^{15}\text{N} \geq 99$ at%, 98.5 %), Maleic acid ($\text{C}_4\text{H}_4\text{O}_4$, ≥ 99.0 %), Deuterium oxide (D_2O , 99 at% D). Milli-Q water ($18.25 \text{ M}\Omega \text{ cm}^{-1}$) was applied across the whole experiments. Before use, Ti mesh was ultrasonically rinsed in acetone, ethanol, and deionized water for 15 minutes to completely remove surface impurities and natural oxides. All the chemicals were used without further purification.

1.2 Synthesis of Pd/CoP.

Here, Pd doped CoP materials were prepared using Ti mesh as a substrate through a two-step hydrothermal and phosphating process. The two-step methods for completing the modification of Ti mesh includes the following steps:

Preparation of precursors: Tilt the Ti mesh into a 35 mL mixed solution containing 0.485 g $\text{Co}(\text{NO}_3)_2 \cdot 6\text{H}_2\text{O}$, 0.155 g NH_4F , 0.5 g $\text{CO}(\text{NH}_2)_2$, and different amounts of Pd sources. After hydrothermal reaction at 120 °C for 6 hours, the precursor catalyst was obtained. After cooling to room temperature, rinse the sample with deionized water three times, and dry it at 60 °C for standby.

Preparation of Pd/CoP with different atomic ratios of Pd: Place the prepared precursor catalyst in a tubular furnace. Subsequently, under argon atmosphere, the sample was roasted at 300 °C for 2h at a heating rate of 2 °C/min to obtain CoP doped with different amounts of Pd. Here, the content of the phosphorus source is 0.2 g.

Preparation of CoP: For pure CoP catalysts, the preparation process is the same as

above, except that no Pd source is added.

1.3 Material characterizations

Scanning electron microscopy (SEM) images were acquired using a Zeiss Supra 40 scanning electron microscope at an acceleration voltage of 5 kV. Transmission electron microscopy (TEM) images were recorded using a JEOL JEM-2010-TEM with an accelerating voltage of 200 kV. The powder X-ray diffraction (XRD) pattern was obtained using a Philips X'Pert PRO SUPER X-ray diffractometer equipped with graphite-monochromated Cu K α radiation ($\lambda = 1.54056 \text{ \AA}$). X-ray photoelectron spectroscopy (XPS) measurement was performed on an X-ray photoelectron 75 spectrometer (ESCALab MKII). The ultraviolet-visible (UV-Vis) absorbance spectra were measured on Shimadzu UV-3900 spectrophotometer. The isotope labeling experiments were measured by ^1H NMR measurement (JNM-ECZ600R). The reaction intermediate information was studied by In-situ Raman spectroscopy (in Via-Reflex).

1.4 Ion concentration detection methods

Colorimetric methods were applied to determine the concentration of nitrate, nitrite, and ammonium.¹ The ultraviolet-visible (UV-Vis) spectrophotometer was used to detect the ion concentration of pre- and post-test electrolytes after diluting to appropriate concentration to match the range of calibration curves.² The specific detection methods are as follow:

Determination of NO_3^- -N: NO_3^- -N concentrations were measured following standard methods. Firstly, a certain amount of electrolyte was taken out from electrolytic cell and diluted to 5 mL in the detected range. Then 100 μL 5 wt% sulfamic acid solution was added into the solution, standing for 10 min at room temperature. The absorption spectrum was tested using an ultraviolet-visible spectrophotometer and the absorption intensities at wavelength of 220 nm and 275 nm were recorded. The final absorbance value was calculated by the equation: $A = A_{220 \text{ nm}} - 2A_{275 \text{ nm}}$. The calibration curve was plotted using a series of concentrations from 0 to 2.50 ppm. And the sodium nitrate applied for plotting calibration curve was pretreated by drying in the oven at 105-110

°C for 2 h in advance.

Determination of NO_2^- -N: A mixture of p-aminobenzenesulfonamide (0.4 g), N-(1-Naphthyl) ethylenediamine dihydrochloride (0.02 g), ultrapure water (5 mL) and phosphoric acid (1 mL, $\rho=1.70$ g/mL) was used as a color reagent. A certain amount of electrolyte was taken out from the electrolytic cell and diluted to 5 mL to detection range. Next, 0.1 mL color reagent was added into the aforementioned 5 mL solution and mixed uniformly, and the absorption intensity at a wavelength of 540 nm was recorded after sitting for 20 min. The concentration-absorbance curve was calibrated using a series of standard sodium nitrite solutions.

Detection of NH_4^+ -N: The Nessler's reagent was prepared by dissolving 0.35 g KI, 0.5 g HgI_2 in 5 mL 4.0 M NaOH solution successively and then the mixed solution was placed in the dark without disturbance for 24 h, finally the liquid supernatant was transferred into a Teflon bottle refrigerated for use. For colorimetric assay, a certain amount of electrolyte was taken out from electrolytic cell and diluted to 5 mL to detection range. Next, 0.1 mL potassium sodium tartrate solution ($\rho = 500$ g L^{-1}) was added and mixed thoroughly, then 0.1 mL Nessler's reagent was put into the solution. The absorption intensity at wavelength of 420 nm was recorded after sitting for 20 min. The concentration-absorbance curve was made using a series of standard ammonium chloride solutions from 0 to 2.50 ppm and the ammonium chloride crystal was dried at 105 °C for 2 h in advance.

1.5. Electrochemical nitrate reduction experiment

The electrochemical nitrate reduction reaction experiments were carried out using a standard three-electrode system in a single-chamber electrolytic cell. The catalyst loaded on Ti mesh, saturated calomel electrode (SCE), and platinum foil were used as the working electrode, reference electrode, and counter electrode, respectively. 0.5 M Na_2SO_4 solution was used as the electrolyte, and a certain concentration of NaNO_3 was added to the electrolytic cell as the target reactant. All the electrochemical measurements were performed using CHI 660E electrochemical workstation (CHI 660E, Chenhua, Shanghai). The potential is recorded under a standard hydrogen

electrode, and the conversion formula is $E_{(RHE)} = E_{(SCE)} + 0.0591 \text{ pH} + 0.2438$. Before conducting the nitrate electroreduction test, the linear sweep voltammetry was performed to make the polarization curve reach a steady state. A constant potential test was carried out at different potentials for 2 hours.

1.6. N isotope labeling experiments

The N isotopic labeling experiments were carried out using the electrochemical nitrate reduction methods in the electrolyte (50 ppm NO_3^- -N) with $\text{Na}^{15}\text{NO}_3$ and $\text{Na}^{14}\text{NO}_3$ as N source, respectively.³ The amount of produced $^{15}\text{NH}_4^+$ -N and $^{14}\text{NH}_4^+$ -N was quantified by the ^1H -Nuclear Magnetic Resonance (NMR) spectroscopy. For quantitative, we prepared a series of standard solutions and plotted the standard curve. First, a series of $^{15}\text{NH}_4^+$ -N solutions with known concentration were prepared in 0.5 M Na_2SO_4 as standards; Second, 50 mL of the $^{15}\text{NH}_4^+$ -N and standard solution with different concentration was mixed with 50 ppm maleic acid; Third, 50 μL deuterium oxide (D_2O) was added in 0.5 mL above mixed solution for the NMR detection; Fourth, the calibration was achieved using the peak area ratio between $^{15}\text{NH}_4^+$ -N and maleic acid because the $^{15}\text{NH}_4^+$ -N concentration and the area ratio were positively correlated. Similarly, the amount of $^{14}\text{NH}_4^+$ -N was quantified by this method when $\text{Na}^{14}\text{NO}_3$ was used as the feeding N-source.

1.7 Assembly of the Zn- NO_3^- battery and electrochemical test.

The Ti mesh-supported Pd/CoP ($1 \times 1 \text{ cm}^2$) and Zn Foil ($1.5 \times 2 \text{ cm}^2$) were employed as the cathode for Zn- NO_3^- battery. A typical H-type cell that contains 30 mL cathode electrolyte (0.5 M Na_2SO_4 + 5 mM NaNO_3 -N) and 30 mL anode electrolyte (1 M KOH) separated by a bipolar membrane (Nafion 117). The discharging polarization curves with a scan rate of 5 mV/s and galvanostatic tests were conducted using CHI 660E workstation at room temperature.

The power density (P) of Zn- NO_3^- battery was determined by $P = I \times V$, where I and V are the discharge current density and voltage, respectively.

The electrochemical reactions in Zn-nitrate battery are presented as following:

Cathode reaction: $\text{NO}_3^- + 7\text{H}_2\text{O} + 8\text{e}^- \rightarrow \text{NH}_4\text{OH} + 9\text{OH}^-$

Anode reaction: $4\text{Zn} + 8\text{OH}^- \rightarrow 4\text{ZnO} + 4\text{H}_2\text{O} + 8\text{e}^-$

Overall reaction: $4\text{Zn} + \text{NO}_3^- + 3\text{H}_2\text{O} \rightarrow 4\text{ZnO} + \text{NH}_4\text{OH} + \text{OH}^-$

1.8 Density functional theory (DFT) calculation

The first-principles were employed to perform all density functional theory (DFT) calculations within the generalized gradient approximation (GGA) using the Perdew-Burke-Ernzerhof (PBE) formulation.^{4,6} The projected augmented wave (PAW) potentials were chosen to describe the ionic cores and take valence electrons into account using a plane wave basis set with a kinetic energy cutoff of 520 eV.^{7,8} Partial occupancies of the Kohn-Sham orbitals were allowed using the Gaussian smearing method and a width of 0.05 eV. The electronic energy was considered self-consistent when the energy change was smaller than 10^{-5} eV. A geometry optimization was considered convergent when the energy change was smaller than $0.05 \text{ eV } \text{\AA}^{-1}$. In our structure, the U correction is used for Pd (4.72 eV) atoms. The vacuum spacing in a direction perpendicular to the plane of the structure is 20 \AA for the surfaces. The Brillouin zone integration is performed using $2 \times 2 \times 1$ Monkhorst-Pack k-point sampling for a structure.

For the structure construction of Pd/CoP and CoP, we use CoP (201) as exposure site for subsequent theoretical calculation. Specifically, the CoP structure had been built with the CoP (201) surface, and the equilibrium lattice constants of unit cell were optimized with, when using a $2 \times 2 \times 1$ Monkhorst-Pack k-point grid for Brillouin zone sampling, to be $a=b=11.93560 \text{ \AA}$, $c=22.87270 \text{ \AA}$, $\alpha=\beta=90^\circ$, $\gamma=120^\circ$. Meanwhile, the CoP structure with Pd doping (Pd/CoP) had been built, which is realized by randomly replacing Co atoms on the surface in CoP structures with Pd atoms. During structural optimizations, a $2 \times 2 \times 1$ k-point grid in the Brillouin zone was used for k-point sampling, and all atoms were allowed to relax.

Finally, the adsorption energies (E_{ads}) were calculated as $E_{\text{ads}} = E_{\text{ad/sub}} - E_{\text{ad}} - E_{\text{sub}}$, where $E_{\text{ad/sub}}$, E_{ad} , and E_{sub} are the total energies of the optimized adsorbate/substrate system, the adsorbate in the structure, and the clean substrate, respectively. The free

energy was calculated using the equation:

$$G = E_{\text{ads}} + \text{ZPE} - TS$$

where G , E_{ads} , ZPE and TS are the free energy, total energy from DFT calculations, zero-point energy and entropic contributions, respectively.

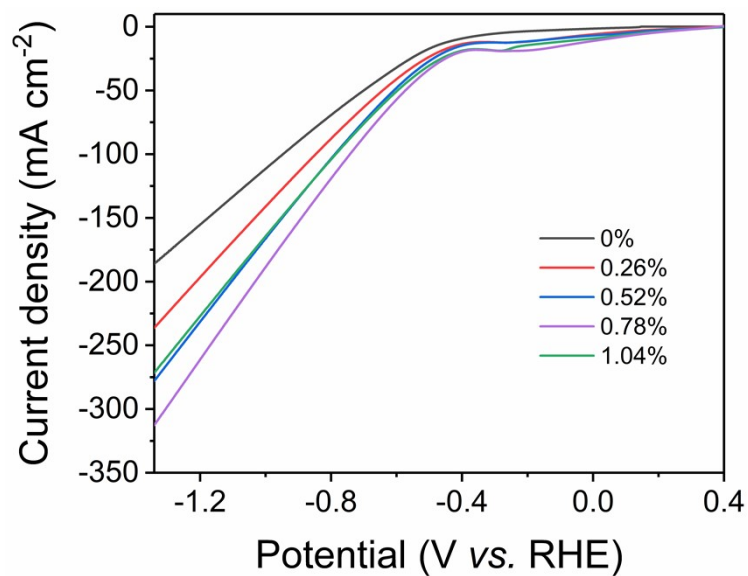


Fig. S1. The LSV curves of Pd/CoP with different atomic ratio Pd.

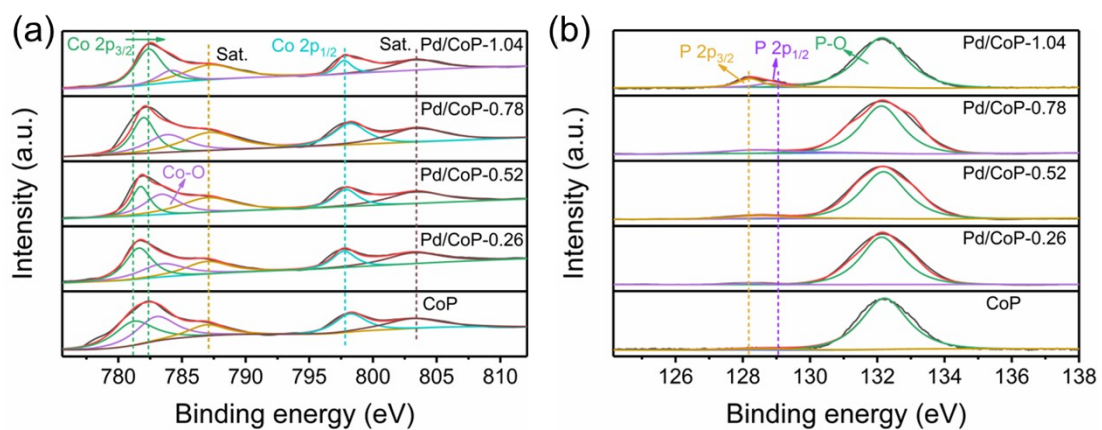


Fig. S2. The XPS spectra of Pd/CoP with different atomic ratio Pd in (a) Co 2p region, (b) P 2p region.

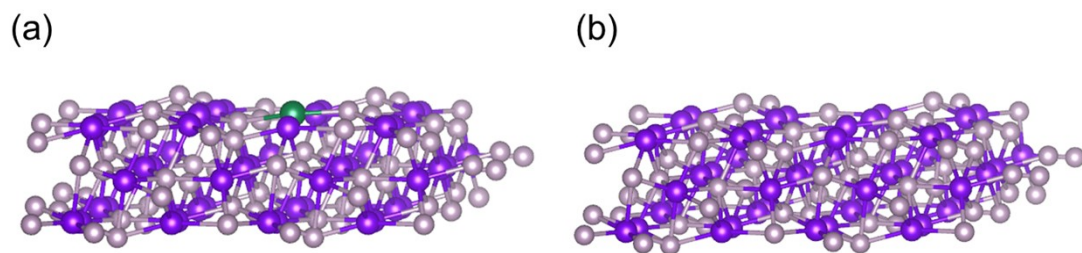


Fig. S3. The optimal structure model of (a) Pd/CoP and (b) CoP.

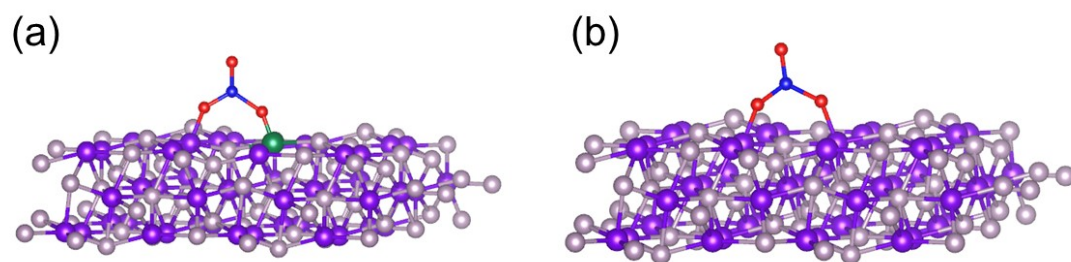


Fig. S4. The optimal structure model of (a) Pd/CoP and (b) CoP after adsorbing NO_3^- .

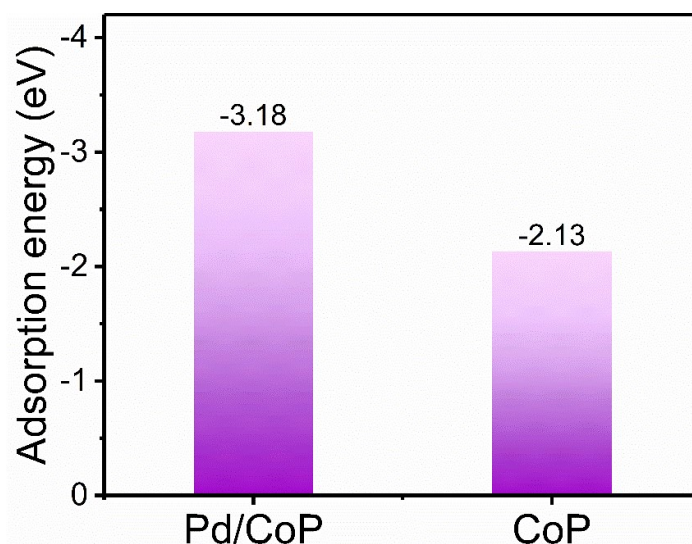


Fig. S5. The adsorption energy of NO_3^- on Pd/CoP and CoP.

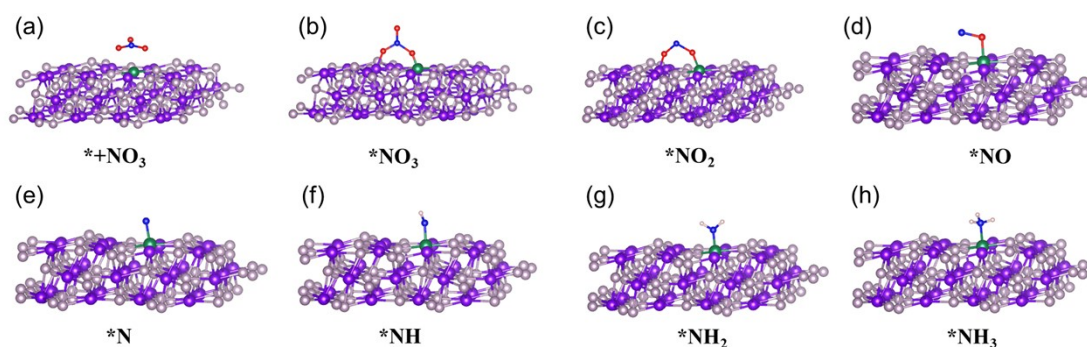


Fig. S6. Pd/CoP configurations and stable configurations of the intermediates on Pd/CoP. The most stable adsorption configurations of $*\text{NO}_3$, $*\text{NO}_2$, $*\text{NO}$, $*\text{N}$, $*\text{NH}$, $*\text{NH}_2$, and $*\text{NH}_3$.

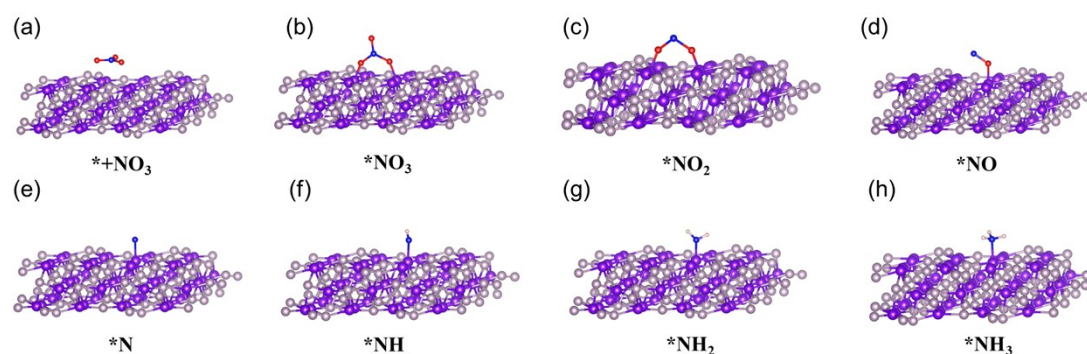


Fig. S7. CoP configurations and stable configurations of the intermediates on CoP. The most stable adsorption configurations of $*\text{NO}_3$, $*\text{NO}_2$, $*\text{NO}$, $*\text{N}$, $*\text{NH}$, $*\text{NH}_2$, and $*\text{NH}_3$.

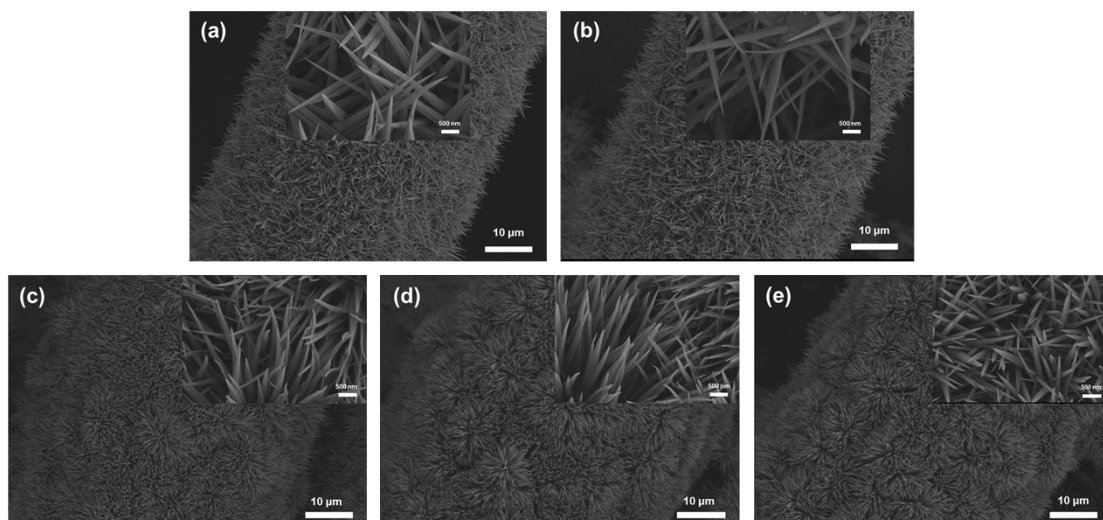


Fig. S8. The SEM images of Pd/CoP with different atomic ratio Pd.

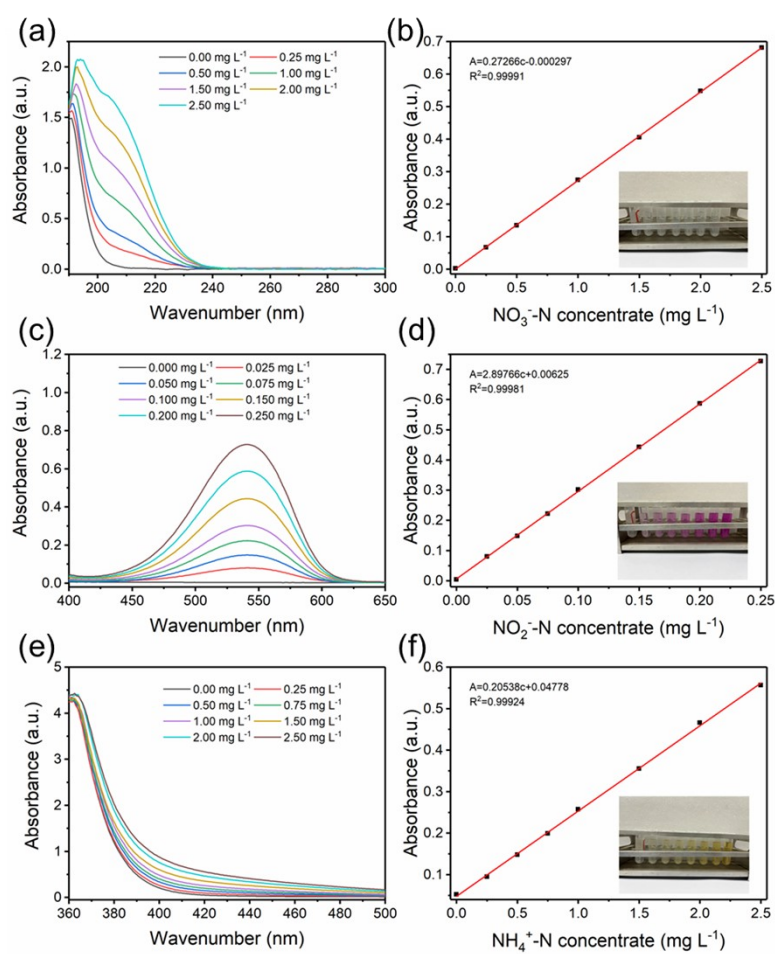


Fig. S9. The concentration-absorbance calibration curves of (a) NO_3^- -N, (b) NO_2^- -N and (c) NH_4^+ -N. The calibration curves all show good linearity.

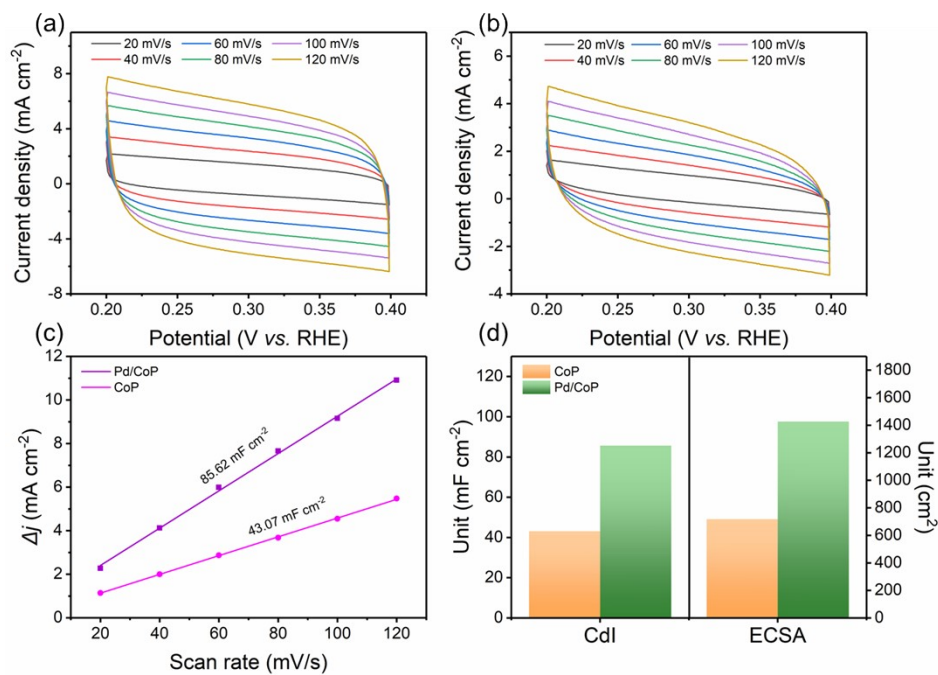


Fig. S10. CV curves of (a) Pd/CoP and (b) CoP samples at different scanning rate. (c) Double-layer capacitance (C_{dl}) of Pd/CoP and CoP samples, (d) C_{dl} and ECSA summary of different samples.

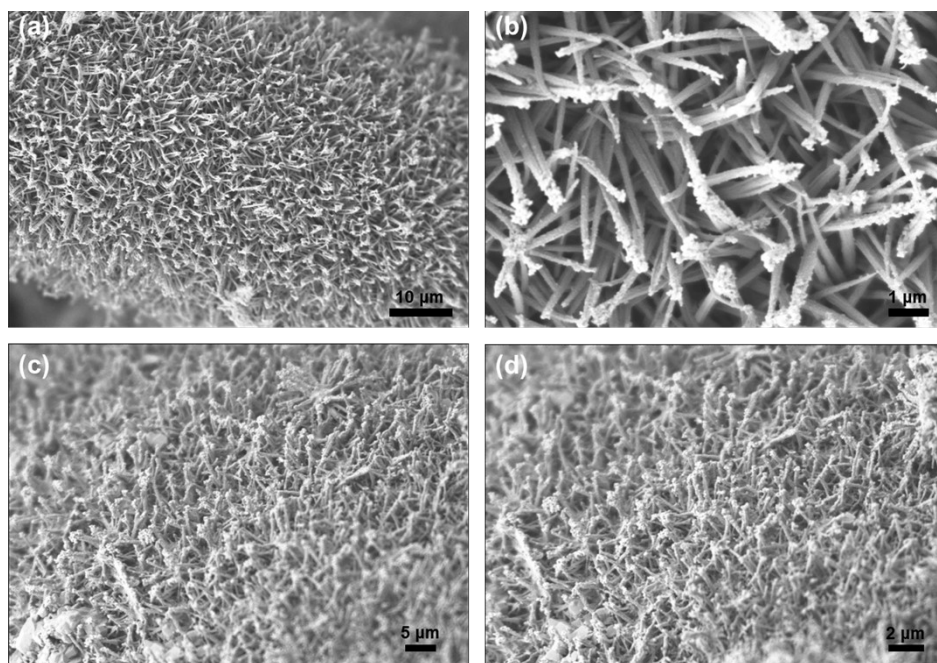


Fig. S11. The SEM images of (a, b) Pd/CoP and (c, d) CoP samples at different magnification after testing.

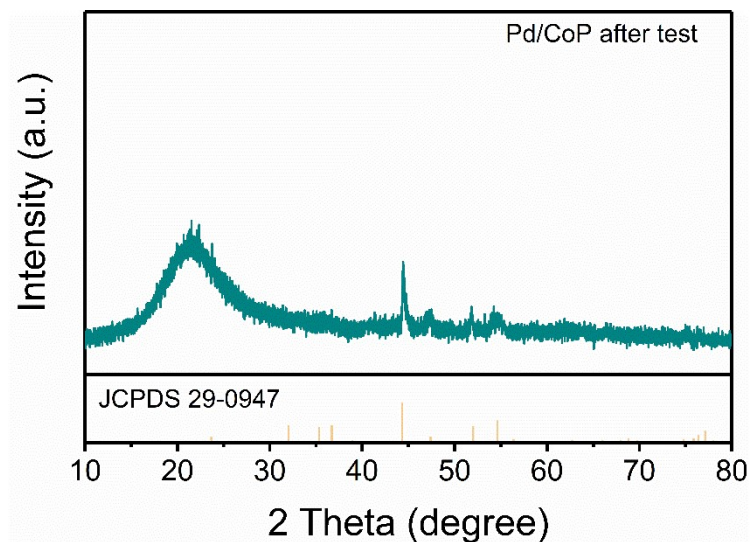


Fig. S12. The XRD pattern of Pd/CoP sample after testing.

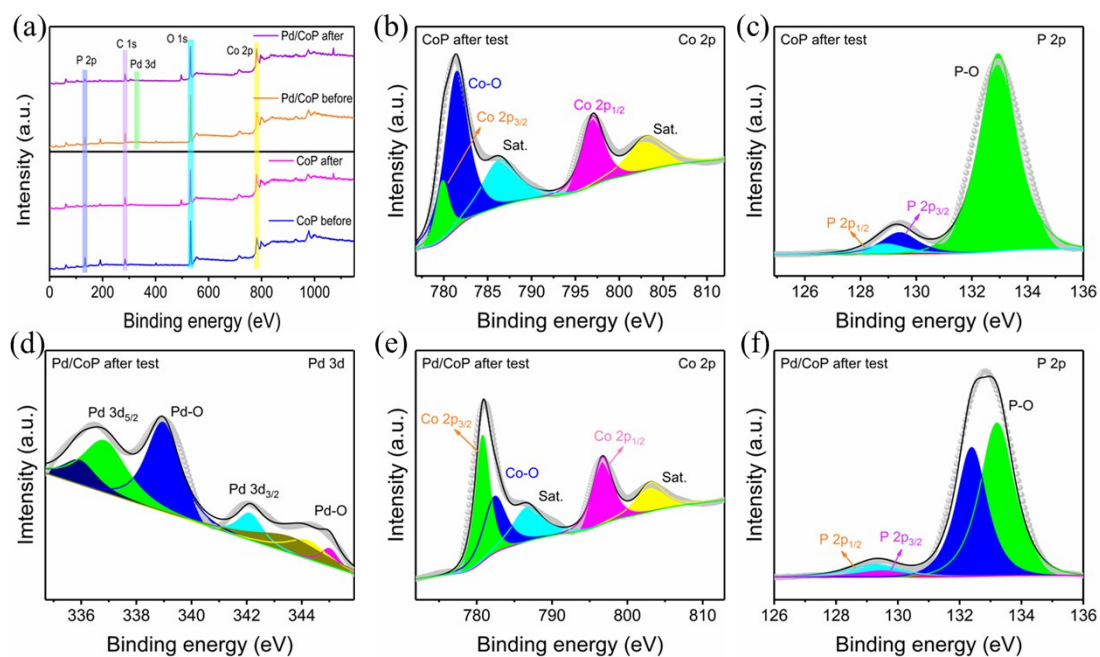


Fig. S13. (a) The XPS all spectra of Pd/CoP and CoP samples after testing. High-resolution (b) Co 2p, (c) P 2p XPS spectra of CoP after testing. High-resolution (d) Pd 3d, (e) Co 2p, (f) P 2p XPS spectra of Pd/CoP after testing.

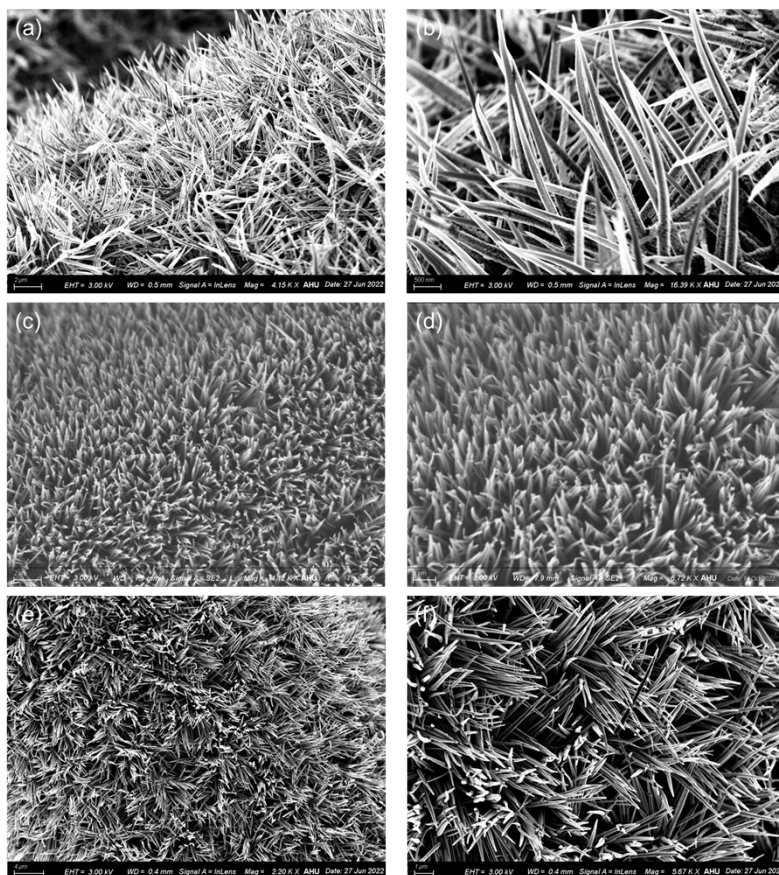


Fig. S14. The SEM images of (a, b) Ni/CoP, (c, d) Fe/CoP, and (e, f) Cu/CoP at different magnification.

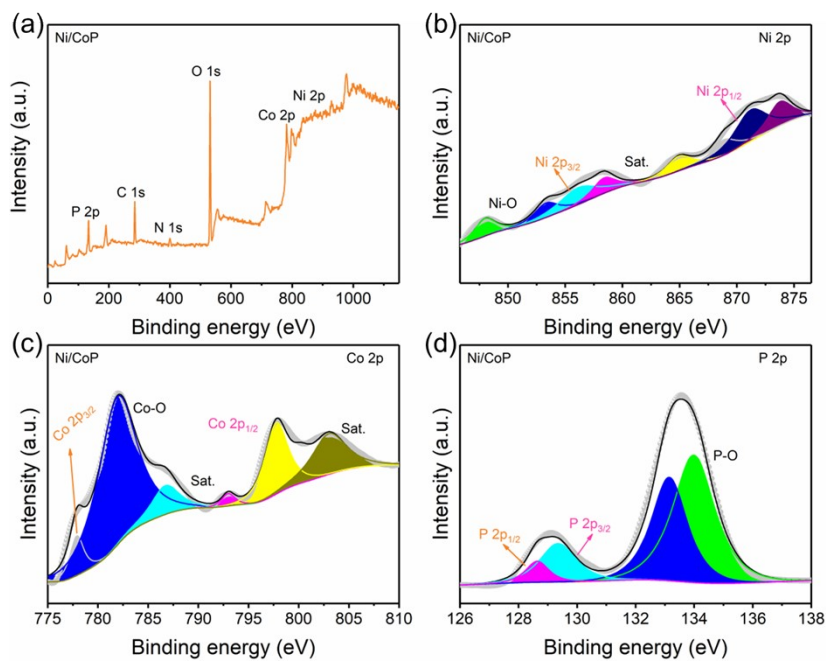


Fig. S15. (a) XPS all spectra; High-resolution (b) Ni 2p, (c) Co 2p, (d) P 2p XPS spectra of Ni/CoP sample.

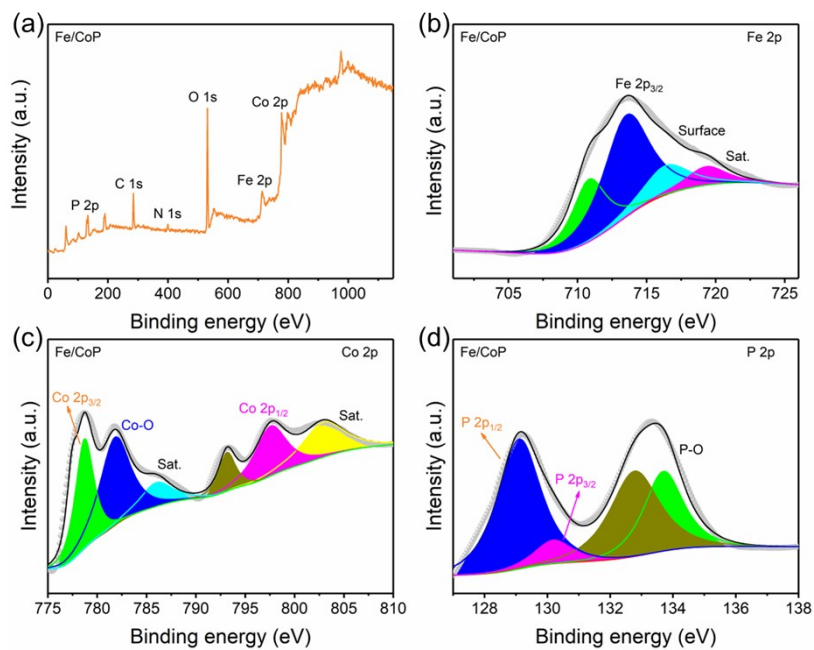


Fig. S16. (a) XPS all spectra; High-resolution (b) Fe 2p, (c) Co 2p, (d) P 2p XPS spectra of Fe/CoP sample.

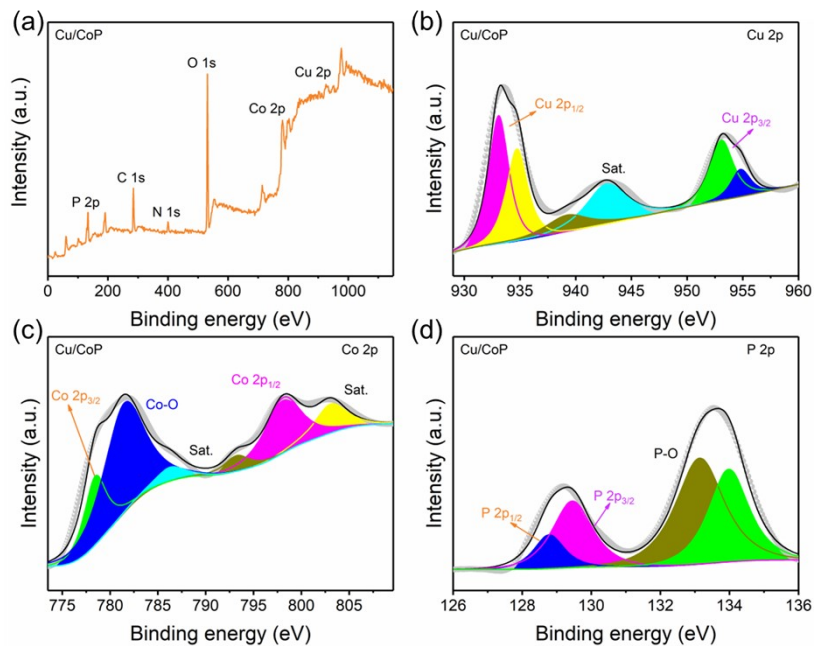


Fig. S17. (a) XPS all spectra; High-resolution (b) Cu 2p, (c) Co 2p, (d) P 2p XPS spectra of Cu/CoP sample.

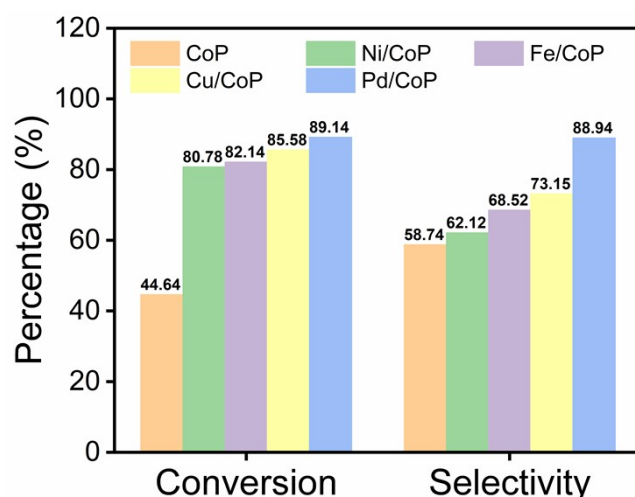


Fig. S18. The NO_3^- -RR performance of metal/CoP.

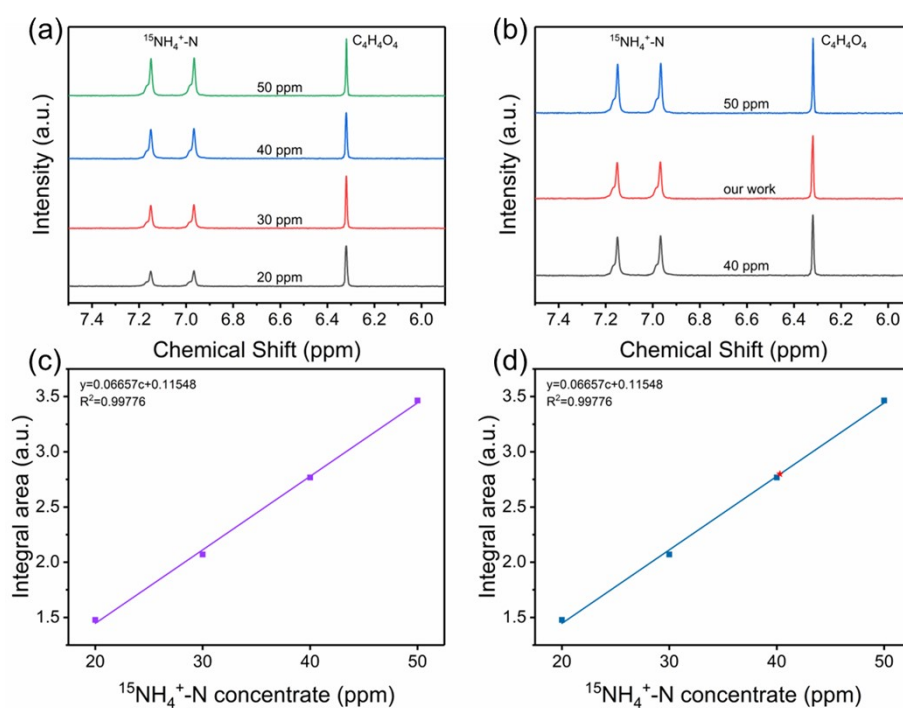


Fig. S19. (a) ^1H NMR spectra (600 MHz) of various $^{15}\text{NH}_4^+$ ion concentration ($^{15}\text{NH}_4^+-\text{N}$) with maleic acid as the reference (300 ppm). (b) Integral area ($^{15}\text{NH}_4^+-\text{N} / \text{C}_4\text{H}_4\text{O}_4$) against $^{15}\text{NH}_4^+-\text{N}$. (c) ^1H NMR spectra (600 MHz) of the electrolyte after $^{15}\text{NO}_3^-$ reduction over Pd/CoP at -0.8 V vs. RHE for 2 h. (d) The $^{15}\text{NH}_4^+-\text{N}$ of the electrolyte that was quantified by ^1H NMR with maleic acid (300 ppm) as the reference.

The proton signal of maleic acid in Na_2SO_4 solution appears at $\delta = 6.29 \text{ ppm}$. The proton signals of $^{15}\text{NH}_4^+-\text{N}$ in Na_2SO_4 solution are observed at $\delta = 6.97 \text{ ppm}$ and $\delta = 7.09 \text{ ppm}$.⁹

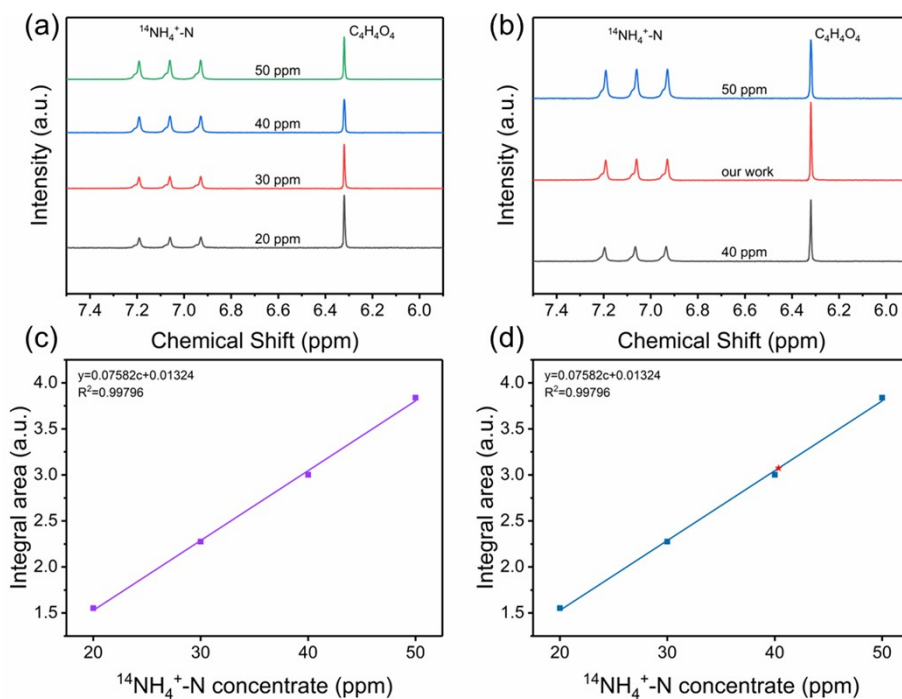


Fig. S20. (a) ^1H NMR spectra (600 MHz) of various $^{14}\text{NH}_4^+$ ion concentration ($^{14}\text{NH}_4^+$ -N) with maleic acid as the reference (300 ppm). (b) Integral area ($^{14}\text{NH}_4^+$ -N / $\text{C}_4\text{H}_4\text{O}_4$) against $^{14}\text{NH}_4^+$ -N. (c) ^1H NMR spectra (600 MHz) of the electrolyte after $^{14}\text{NO}_3^-$ reduction over Pd/CoP at -0.8 V vs. RHE for 2 h. (d) The $^{14}\text{NH}_4^+$ -N of the electrolyte that was quantified by ^1H NMR with maleic acid (300 ppm) as the reference.

The proton signal of maleic acid in Na_2SO_4 solution appears at $\delta = 6.29$ ppm. The proton signals of $^{14}\text{NH}_4^+$ -N in Na_2SO_4 solution are observed at $\delta = 6.94$ ppm, $\delta = 7.03$ ppm and $\delta = 7.12$ ppm.⁹

Table S1. Pd/CoP XPS atom percentage.

Element	Peak Binding Energy (eV)	Atom %
C 1s	284.8	37.54
C 1s Scan A	286.29	8.86
C 1s Scan B	288.34	4.85
Co 2p	782	21.39
P 2p	133.69	27.06
Pd 3d	336.33	0.31

Table S2. CoP XPS atom percentage.

Element	Peak Binding Energy (eV)	Atom %
C 1s	284.8	40.23
C 1s Scan A	286.49	6.09
C 1s Scan B	288.67	2.97
Co 2p	782	19.37
P 2p	134.01	31.34

Table S3. The C_{dl} and ECSA of Pd/CoP and CoP samples.

Samples	C_{dl} (mF cm ⁻²)	ECSA (cm ²)
Pd/CoP	85.62	1426.43
CoP	43.07	717.55

Here, the reference value of the surface double-layer capacitance is 16.67 $\mu\text{F cm}^{-2}$

Table S4. Comparison of the different quantitative methods.

Quantitative methods	Detected ion	Concentration (ppm)	Yield rate (mmol h ⁻¹ cm ⁻²)
Colorimetric method	¹⁴ NH ₄ ⁺ -N	39.64	0.099
¹ H NMR	¹⁴ NH ₄ ⁺ -N	41.18	0.10287
¹ H NMR	¹⁵ NH ₄ ⁺ -N	40.17	0.10035

Table S5. Performance comparison of the well-developed catalysts for NO₃⁻RR.

Catalysts	Faradaic efficiency (%)	Yield rate (mmol h⁻¹ cm⁻²)	Ref.
Co-Fe/Fe ₂ O ₃	30	0.015	10
Fe/Fe ₃ O ₄	32	0.00553	11
RuO ₂ /Ti	52.1	0.0193	12
Pd-Cu/C	62.3	0.1104	13
PTCDA/O-Cu	77	0.0311	14
Co ₃ O ₄ /Ti	80	0.0453	15
Cu@Cu ₂ O	81.2	0.01166	16
Pd/TiO ₂	92.05	0.07994	17
Pd/CoP	82.46	0.099	This work

Table S6. Performance comparison of the well-developed catalysts for Zn-NO₃⁻ battery.

Catalysts	Faradaic efficiency (%)	Yield rate (μmol h⁻¹ cm⁻²)	Ref.
Fe/Ni ₂ P	81.3	5.1	18
Fe/Co ₃ O ₄	60	2.784	19
Pd/TiO ₂	45.3	14.28	17
NiCo ₂ O ₄ /CC	51.37	9.8	20
CoNi-Vp	76.23	9.5233	21
Co ₂ AlO ₄	82.5	3.569	22
Pd/CoP	86.76	12.176	This work

References

1. R. Mao, H. Zhu, K. Wang and X. Zhao, *Appl. Catal. B Environ.*, 2021, **298**, 120552.
2. X. Cui, C. Tang and Q. Zhan, *Adv. Energy Mater.*, 2018, **8**, 1800369.
3. X. Fu, C. Shang, G. Zhou and X. Wang, *J. Mater. Chem. A*, 2021, **9**, 24963–24970.
4. G. Kresse and J. Furthmüller, *Comp. Mater. Sci.*, 1996, **6**, 15-50.
5. G. Kresse and J. Furthmüller, *Phys. Rev. B*, 1996, **54**, 169-186.
6. J. P. Perdew, K. Burke and M. Ernzerhof, *Phys. Rev. Lett.*, 1996, **77**, 3865-3868.
7. G. Kresse and D. Joubert, *Phys. Rev. B*, 1999, **59**, 1758-1775.
8. P. E. Blochl, *Phys. Rev. B*, 1994, **50**, 17953-17979.
9. X. Cui, C. Tang and Q. Zhang, *Adv. Energy Mater.*, 2018, **8**, 1800369.
10. S. Zhang, M. Li, J. Li, Q. Song and X. Liu, *Proc. Natl. Acad. Sci. U.S.A.*, 2022, **119**, e2115504119.
11. Z. A. Jonoush, A. Rezaee and A. Ghaffarinejad, *J. Clean. Prod.*, 2020, **242**, 118569.
12. L.-K. Wu, Y.-J. Shi, C. Su, H.-Z. Cao and G. Q. Zheng, *Catal. Lett.*, 2019, **149**, 1216–1223.
13. Z. Wang, C. Sun, X. Bai, Z. Wang, X. Yu, X. Tong, Z. Wang, H. Zhang, H. Pang, L. Zhou, W. Wu, Y. Liang, A. Khosla and Z. Zhao, *ACS Appl. Mater. Interfaces*, 2022, **14**, 30969-30978.
14. G.-F. Chen, Y. Yuan, H. Jiang, S.-Y. Ren, L.-X. Ding, L. Ma, T. Wu, J. Lu and H. Wang, *Nat. Energy*, 2020, **5**, 605-613.
15. J. Gao, B. Jiang, C. Ni, Y. Qi, Y. Zhang, N. Oturan and M. A. Oturan, *Appl. Catal. B Environ.*, 2019, **254**, 391-402.
16. Y. Wang, W. Zhou, R. Jia, Y. Yu and B. Zhang, *Angew. Chem. Int. Ed.*, 2020, **59**, 5350-5354.
17. Y. Guo, R. Zhang, S. Zhang, Y. Zhao, Q. Yang, Z. Huang, B. Dong and C. Zhi, *Energy Environ. Sci.*, 2021, 3938–3944.
18. R. Zhang, Y. Guo, S. Zhang, D. Chen, Y. Zhao, Z. Huang, L. Ma, P. Li, Q. Yang, G. Liang and C. Zhi, *Adv. Energy Mater.*, 2022, **12**, 2103872.
19. P. Wei, J. Liang, Q. Liu, L. Xie, X. Tong, Y. Ren, T. Li, Y. Luo, N. Li, B. Tang, A. M. Asiri, M. S. Hamdy, Q. Kong, Z. Wang and X. Sun, *J. Colloid Interface Sci.*, 2022, **615**, 636-642.
20. Q. Liu, L. Xie, J. Liang, Y. Ren, Y. Wang, L. Zhang, L. Yue, T. Li, Y. Luo, N. Li, B. Tang, Y. Liu, S. Gao, A. A. Alshehri, I. Shakir, P. O. Agboola, Q. Kong, Q. Wang, D. Ma and X. Sun, *Small*, 2022, **18**, 2106961.
21. Y. Gao, K. Wang, C. Xu, H. Fang, H. Yu, H. Zhang, S. Li, C. Li and F. Huang, *Appl. Catal. B Environ.*, 2023, **330**, 122627.
22. Z. Deng, J. Liang, Q. Liu, C. Ma, L. Xie, L. Yue, Y. Ren, T. Li, Y. Luo, N. Li, B. Tang, A. A. Alshehri, I. Shakir, P. O. Agboola, S. Yan, B. Zheng, J. Du, Q. Kong and X. Sun, *Chem. Eng. J.*, 2022, **435**, 135104.